Astronomy & Astrophysics manuscript no.
(will be inserted by hand later)

Radio continuum spectra of galaxies in the Virgo cluster region⋆

B. Vollmer[1,2], M. Thierbach[2], & R. Wielebinski[2]

[1] CDS, Observatoire astronomique de Strasbourg, UMR 7550, 11, rue de l'université, 67000 Strasbourg, France
[2] Max-Planck-Institut für Radioastronomie, Auf dem Hügel 69, 53121 Bonn Germany

Received / Accepted

Abstract. New radio continuum observations of galaxies in the Virgo cluster region at 4.85, 8.6, and 10.55 GHz are presented. These observations are combined with existing measurements at 1.4 and 0.325 GHz. The sample includes 81 galaxies were spectra with more than two frequencies could be derived. Galaxies that show a radio–FIR excess exhibit central activity (HII, LINER, AGN). The four Virgo galaxies with the highest absolute radio excess are found within 2° of the center of the cluster. Galaxies showing flat radio spectra also host active centers. There is no clear trend between the spectral index and the galaxy's distance to the cluster center.

Key words. Galaxies: clusters: individual: Virgo – Galaxies: evolution – Galaxies: magnetic fields – Radio continuum: galaxies Galaxies:

1. Introduction

A galaxy cluster is an ideal laboratory for studying the influence of the galaxies' environment on its appearance and/or evolution. It is a well established fact that spiral galaxies in clusters have less atomic gas than isolated spirals of the same morphological type and same optical diameter, i.e. they are HI deficient (Chamaraux et al. 1980, Bothun et al. 1982, Giovanelli & Haynes 1985, Gavazzi 1987, 1989). There are mainly two kinds of mechanisms which are able to cause the removal of the atomic gas: (i) tidal interactions or (ii) the interaction of the interstellar medium (ISM) with the hot intracluster medium (ICM). The mapping of the gas content of spiral galaxies in the Virgo cluster (Cayatte et al. 1990, 1994) showed that the HI disk sizes of cluster spirals are considerably reduced. In addition, galaxies with a symmetric optical disk that have an asymmetric HI gas distribution are quite frequent in the cluster core. These observational results indicate that the gas removal due to the rapid motion of the galaxy within the ICM (ram pressure stripping; Gunn & Gott 1972) is responsible for the HI deficiency and the distorted gas disks of the cluster spirals.

During the phase of active ram pressure stripping the interstellar matter (ISM), which is located in the outer disk is pushed to smaller radii where it is compressed (Vollmer et al. 2001). This effect is more important for edge-on stripping than for face-on stripping. Since the magnetic field is frozen into the ISM, the magnetic field B becomes compressed too and its strength is enhanced (Otmianowka-Mazur & Vollmer 2003). The radio continuum emission due to relativistic particles gyrating around the magnetic fields is proportional to B^{2-4} depending on the fact if there is equipartition between the relativistic electrons and the magnetic field. One might thus expect an enhancement of the radio continuum emission of spiral galaxies that undergo active ram pressure stripping. This enhancement should be detectable as a radio excess in the well studied radio–FIR correlation (see, e.g., de Jong et al. 1985, Wunderlich et al. 1987, Niklas 1997).

Furthermore, one might speculate that ram pressure stripping triggers nuclear activity. Since radio spectra of centrally active galaxies (HII, LINER, AGN) are generally flatter than the synchrotron spectra of normal galaxies (mean spectral index $\alpha \sim -0.7$, Israel & van der Hulst 1983), one might expect flatter radio spectra close to the cluster center.

Gavazzi & Boselli (1999a) studied the radio luminosity function of Virgo cluster galaxies for early and late type galaxies separately. They found that late type galaxies develop radio sources with a probability proportional to their optical luminosity, independently of their detailed Hubble type. In a second paper Gavazzi & Boselli (1999b) compared the radio luminosity functions of galaxies in different clusters to those of isolated galaxies. They concluded that the radio luminosity function of Virgo cluster galaxies is consistent with that of isolated galaxies, whereas the Coma cluster galaxies show an excess of radio emissivity.

Send offprint requests to: B. Vollmer, e-mail: bvollmer@astro.u-strasbg.fr

⋆ Based on observations with the 100-m telescope of the MPIfR (Max-Planck-Institut für Radioastronomie) at Effelsberg

Niklas et al. (1995) investigated the behaviour of the radio–FIR correlation and the radio spectra in the Virgo cluster. They claim that galaxies that show an excess of radio emission are located close to the cluster center, whereas the spectra do not seem to be affected by the location of the galaxies in the cluster.

In this article we extend the galaxy sample of Niklas et al. (1995) in adding observations at 8.6 GHz and in enlarging the sample to 81 galaxies, which were observed at 10.55, 8.6, 4.85 GHz with the Effelsberg 100-m telescope. Our data is complemented with 1.4 GHz flux densities from the NVSS where advantage is taken of the NVSS images to check for source confusion and to estimate the correct source flux.

This article has the following strucutre: The sample and the observations are presented in Sec. 2 and Sec. 3. We show the results in Sec. 4 and investigate the radio–FIR correlation in Sec. 5. The distribution of the radio spectra are studied in Sec. 6 followed by the discussion and our conclusions (Sec. 7).

2. The sample

Gavazzi & Boselli (1999a) derived the radio luminosity function of the Virgo cluster by cross-correlating optical data of the Virgo Cluster Catalogue (VCC) (Binggeli et al. 1985) with NVSS radio survey carried out at the VLA at 1.4 GHz (Condon et al. 1998). The 180 positive radio-optical matches that they found build the bases of our survey. We restrict ourselves to radio sources with 1.4 GHz flux densities greater than 10 mJy, which corresponds to a flux density at 10.5 GHz of 2 mJy, assuming a spectral index $\alpha = -0.8$, where

$$S \propto \nu^{\alpha} \tag{1}$$

(S is the radio flux density and ν the frequency). We thus observed 81 galaxies of various Hubble types. Their distribution on the sky is shown in Fig. 1. The number of galaxies of different types are listed in Tab. 1. As expected, the sample is clearly dominated by late type galaxies (Sc/Scd) with a high star formation rate. There are also 10 dwarf galaxies in our sample. We took the λ20, 50 cm flux densities, and the IRAS FIR fluxes from the Goldmine database[1] and the position angle of the galactic disks from LEDA [2]. The FIR flux is calculated according to Helou et al. (1988) in the following way:

$$FIR = 2.58 S_{60_\mu} + S_{100_\mu} \ , \tag{2}$$

where S_{60_μ} is the flux at 60 μm and S_{100_μ} the flux at 100 μm.

Fig. 2 shows the number of galaxies as a function of the corrected B band magnitude in bins of 0.5 mag. For comparison, the complete sample of Virgo galaxies brighter than m_B=18 (Gavazzi & Boselli 1999a) is also shown. Most of the missing galaxies in our sample compared to that of Gavazzi & Boselli (1999a) have photographic magnitudes around m_B=12 and m_B=14.

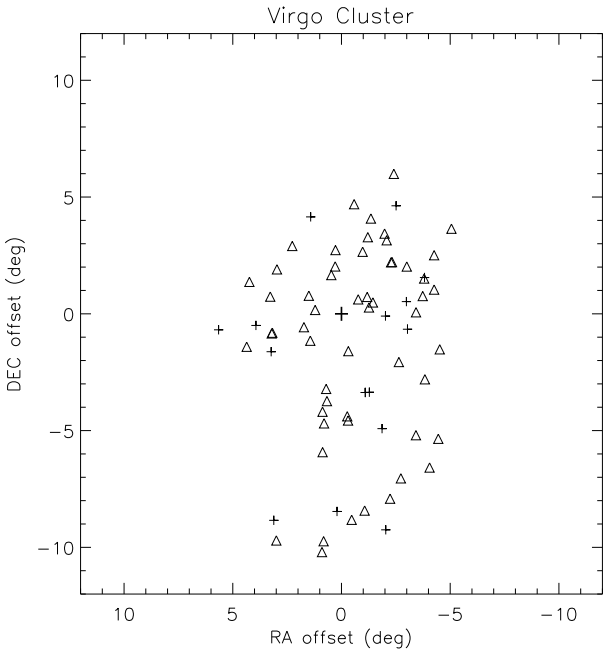

Fig. 1. Distribution of the observed galaxies. Triangles: Virgo galaxies. Crosses: background galaxies. Thick cross: M87.

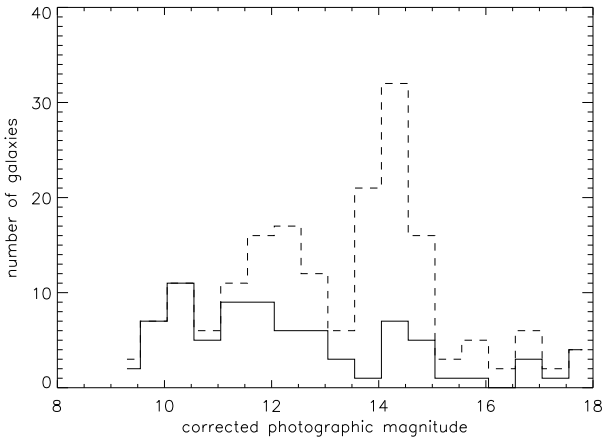

Fig. 2. Number of galaxies as a function of the corrected B band magnitude in bins of 0.5 mag. Solid: our sample. Dashed: complete sample of Virgo galaxies brighter than m_B=18 (Gavazzi & Boselli 1999a).

3. Observations

Our sample of 81 galaxies was observed November 2000, January 2001, August/September/November 2002, and April/June 2003 with the 100-m Effelsberg telescope at 4.85, 8.6, and 10.55 GHz (6.0, 3.6, and 2.8cm). The

[1] This research has made use of the GOLDMine Database, which is operated by the University of Milano-Bicocca (see Gavazzi et al. 2003, A&A, 400, 451)

[2] HyperLeda is an extragalactic database located at http://leda.univ-lyon1.fr/

Table 1. The galaxy sample: number of galaxies per Hubble type.

E/S0	S	Sa/Sab	Sb/Sbc	Sc/Scd	Sm/Im	Pec	dE	BCD
12	2	10	10	33	2	2	8	2

Table 2. Observations characteristics

Frequency (GHz)	HPBW ($''$)	$T_{\rm sys}$ (K)	bandwidth (GHz)	beams
4.85	147	9	0.5	2
8.6	85	4	1.2	1
10.55	69	50	0.3	4

frequency, HPBW, system temperature, bandwidth, and number of beams are listed in Tab. 2. The existence of several beams at 4.85 and 10.55 GHz permits to subtract nonlinear baselevels due to meteorologic conditions. The most sensitive receiver is the one at 8.6 GHz due to its huge bandwidth and low system temperature. Since it is a single beam receiver, perfect weather conditions are needed for observations at this frequency.

The galaxies were measured with cross-scans. The cross-scans were centered on the radio center of the galaxies given by Gavazzi & Boselli (1999a). The scanning directions were along the major and minor axis of the galaxies. The length of the cross-scans were $16'$, $15'$, and $10'$, the duration of the scan 24, 30, and 30 sec at 4.85, 8.6, and 10.55 GHz respectively. The number of cross-scans and thus the total integration time at a given frequency was calculated using the expected flux density extrapolated from the NVSS flux at 1.4 GHz ($\alpha = -0.8$) and a S/N of 5. The calibration scale for the fluxes is that of Ott et al. (1994). For a correct calibration of the cross-scans and telescope pointing 3C286 was observed frequently during the observations.

In order to derive the flux densities of the cross-scanned galaxies, Gaussians were fitted to the averaged scans in each direction. These fits give the peak flux value $S^{\rm peak}$ and the half-power width $HPW^{\rm obs}$ of the fitted Gaussian and the positional offset. The peak value of each scan direction was then corrected using the following formula to obtain the total flux density $S_{\rm tot}$:

$$S_{\rm tot} = S_1^{\rm peak} \times S_2^{\rm peak} \times (\frac{HPW_1^{\rm obs}}{HPBW}) \times (\frac{HPW_2^{\rm obs}}{HPBW}) \ , \qquad (3)$$

where $S_i^{\rm peak}$ and $HPW_i^{\rm obs}$ with $i = 1, 2$ are the flux densities and half-power widths along the major and minor axis of the galaxies. For the determination of the source extent, the 10.55 GHz and 8.6 GHz data are best suited, because they have the highest resolutions. Unfortunately, meteorological conditions and frequent source confusion did us not allow to derive reliable half-power widths from our data. Therefore, we used our peak fluxes and the half power widths at 1.4 GHz given by Gavazzi & Boselli (1999a).

Source confusion is a serious problem in the Virgo cluster region, especially at 4.85 GHz. Our advantage is that we have the NVSS 1.4 GHz fluxes, where the correct source has been identified on the NVSS images (Gavazzi & Boselli 1999a). Thus, it was possible to identify the confusing source, to subtract it, and to fit a Gaussian to the radio source belonging to the correct VCC source. Since Niklas et al. (1995) did not have the NVSS flux densities they could not decide which source was the correct one. Thus we had to re-observe several of their measured galaxies.

4. Results

The observed flux densities at 4.85, 8.6, and 10.55 GHz are listed in Tab. 3. We have also included the measurements of Niklas et al. (1995), which are marked in boldface. The columns of Tab. 3 are: (1) VCC name of the galaxy (2) right ascension in B1950 coordinates (3) declination in B1950 coordinates (4) projected distance from the Virgo cluster center (M87) (5) Hubble type (6) Virgo cluster membership based on radial velocities (y/n) (7) flux density at 10.55 GHz (8) flux density at 8.6 GHz (9) flux density at 4.85 GHz (10) flux density at 1.4 GHz (11) flux density at 0.6 GHz.(12) FIR flux (see Eq. 2) (13) spectral index α (see Eq. 1). When we did not detect a galaxy at 4.85, 8.6, and 10.55 GHz the upper limit of the flux density is ~ 1 mJy at 10.55 GHz.

We made linear fits in the $\log \nu - \log S_\nu$ plane using the method of the least absolute deviation. This method is less sensitive to outlying points in the spectrum and thus more robust than a χ^2 fit. The obtained spectra are shown in Fig. 3. The spectral index α is plotted in the lower left corner of the boxes. We only fitted a spectrum when there are more than two data points.

Since the cross-scan method is less accurate than imaging of the sources, the spectra are noisier than those obtained by direct imaging. The main error is due to offsets in the Gaussian fits and imprecise position angles of the galaxies. In many cases the flux densities at 10.55 GHz are lower than expected by our fitted spectrum. This might be due to the fact that this receiver is the least sensitive of the three receivers used. Moreover, the background subtraction using a second beam has the effect that the total flux might be underestimated.

5. The radio–FIR correlation

In Fig. 4(a)–(d) and (f) we show the radio–FIR correlation for radio frequencies 10.55, 8.6, 4.85, 1.4, and 0.6 GHz including all galaxies of the sample. The early type galaxies (E) of our sample are marked as triangles. Only one elliptical appears in Fig. 4(a) and (b), because there are no FIR flux densities measured for the other Virgo early type galaxies. Thus, the sample we use here is made of spiral (Sa-Im) and S0 galaxies except VCC0763. The least absolute deviation fits are also shown as solid lines whose slopes are plotted in the lower left corners of the boxes.

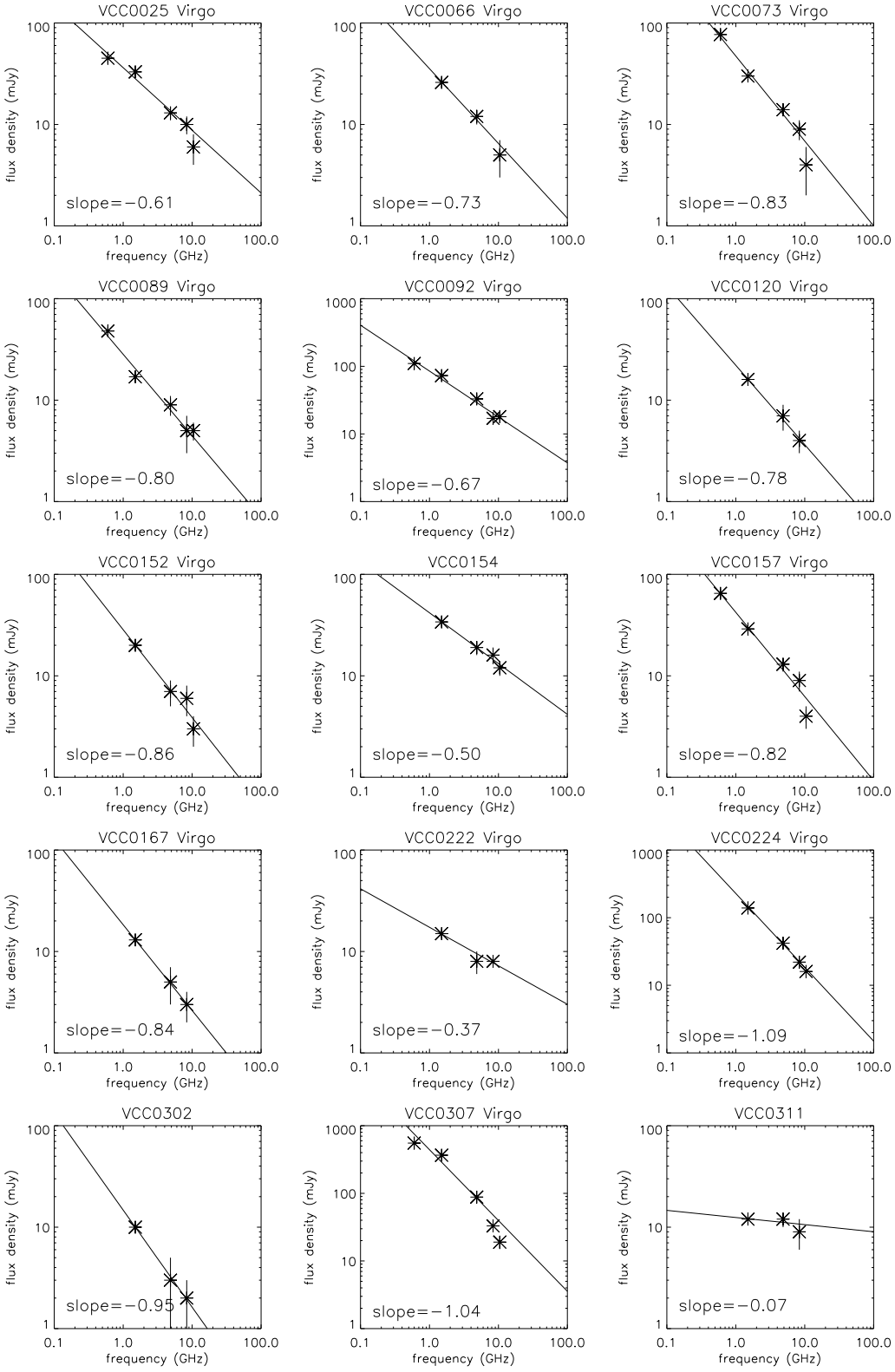

Fig. 3. Radio spectra of the observed VCC sources.

The major outlying galaxies are labeled. In order to investigate if the radio excess of these outliers is located in the disk or in the center of the galaxies, we subtracted the FIRST 1.4 GHz flux densities for sources where the FIRST image shows a central point source (the FIRST resolution is 6″). The radio–FIR correlation using these corrected 1.4 GHz flux densities can be seen in Fig. 4(e). Clearly, the radio excesses are due to central point sources, i.e central activity (LINER, HII, AGN). The slopes of the radio–FIR correlation at 4.85 and 1.4 GHz are consistent

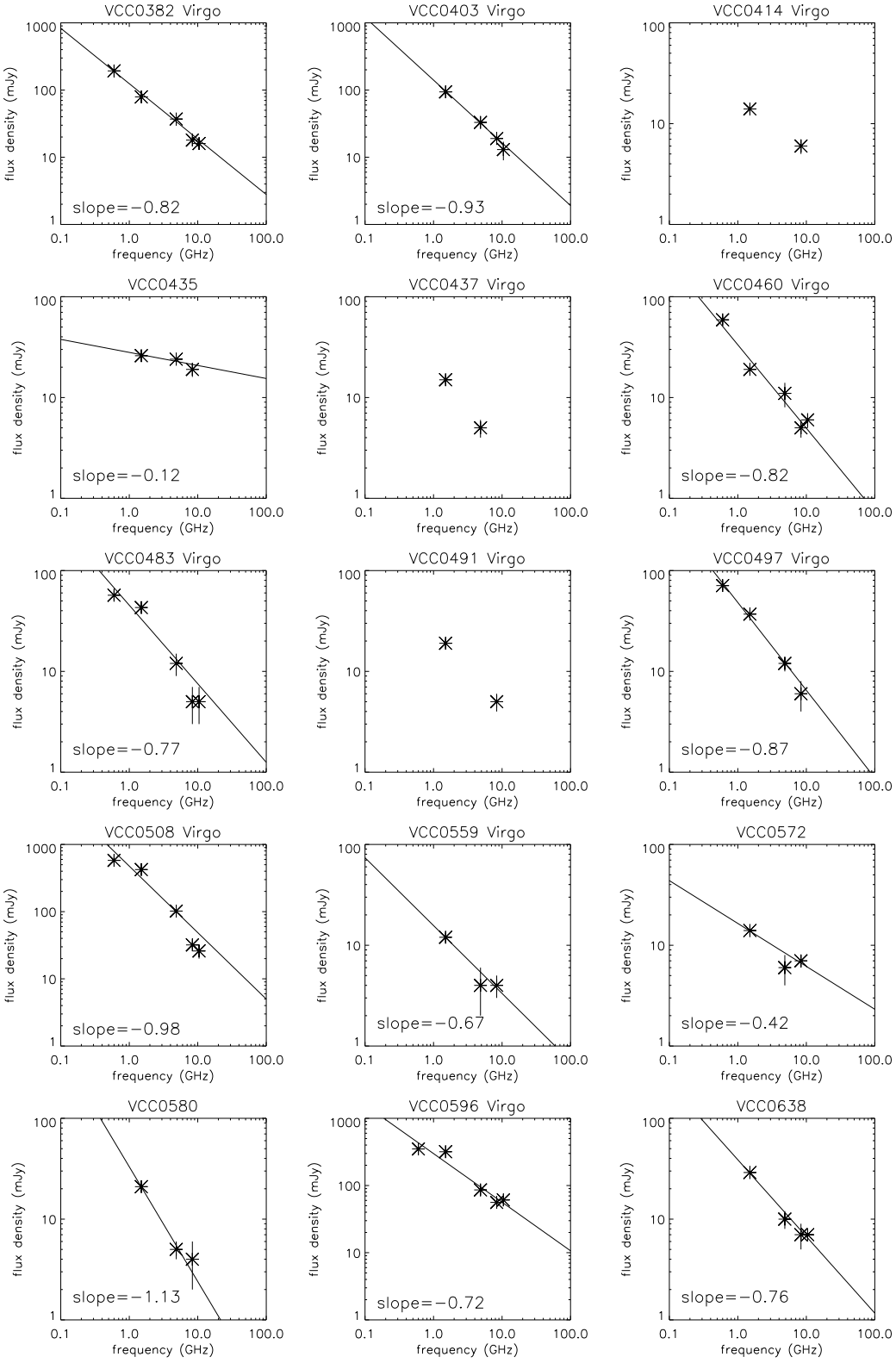

Fig. 3. Radio spectra of the observed VCC sources (continued).

with those of samples of isolated galaxies (Wunderlich et al. 1987, Niklas 1997). At 10.55 GHz our radio data is quite noisy, but when one removes the outlying points the slope is consistent with that found by Niklas et al. (1995) and Niklas (1997). The radio–FIR correlations at 8.6 and 0.6 GHz fit also in this picture.

In order to investigate the location of the Virgo galaxies that show a strong absolute radio excess within the cluster, Fig. 5 shows the absolute radio excess at

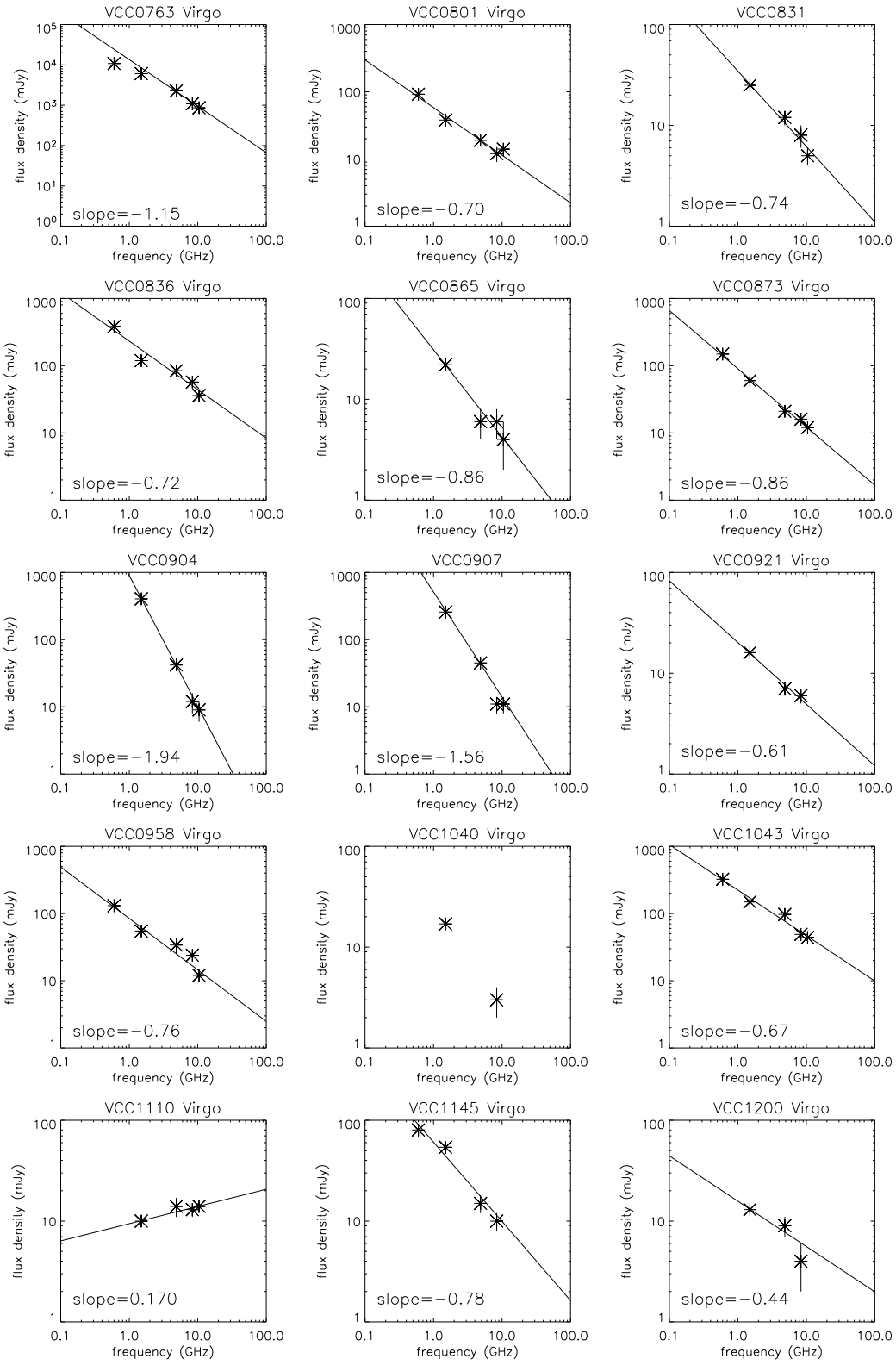

Fig. 3. Radio spectra of the observed VCC sources (continued).

4.85 GHz $S_{4.85\ \mathrm{GHz}} - S_{\mathrm{FIR}}$ as a function of the projected distance to the cluster center (M87). The radio excess is defined as the difference between the observed and the from the radio-FIR correlation expected radio flux. All shown galaxies are classified as spiral or S0 galaxies. We use the measurements at 4.85 GHz, because they are our most accurate measurements. The 4 galaxies that have the highest absolute radio excesses are located at projected distances smaller than 2 degrees ($\sim$ 0.6 Mpc) and are labeled in Fig. 5. All four galaxies

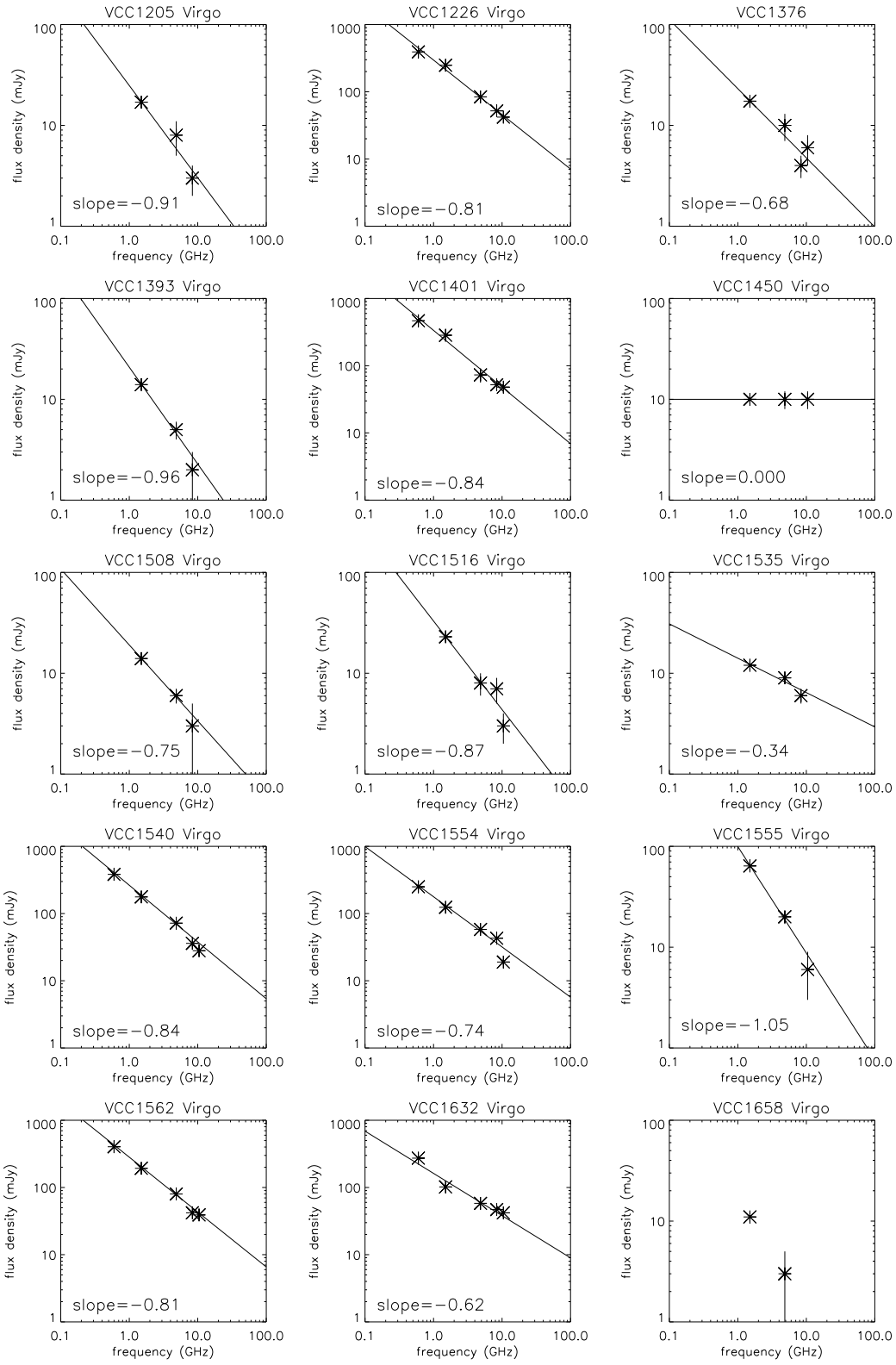

Fig. 3. Radio spectra of the observed VCC sources (continued).

are classified as centrally active (VCC0836 (NGC 4388): Sy2, VCC1043 (NGC 4388): Sy/LINER, VCC1632 (NGC 4552): LINER/HII, VCC1727 (NGC 4579): Sy2/LINER). In addition, VCC0836, VCC1043, and VCC1727 galaxies show extended radio emission. In the case of VCC1043 the radio emission, which is not due to a jet, is even extraplanar (Kotanyi et al. 1983). But as can be seen in Fig. 4(e), when one subtracts the flux density of the FIRST central point sources, there is no more radio excess observed. We have also calculated the relative

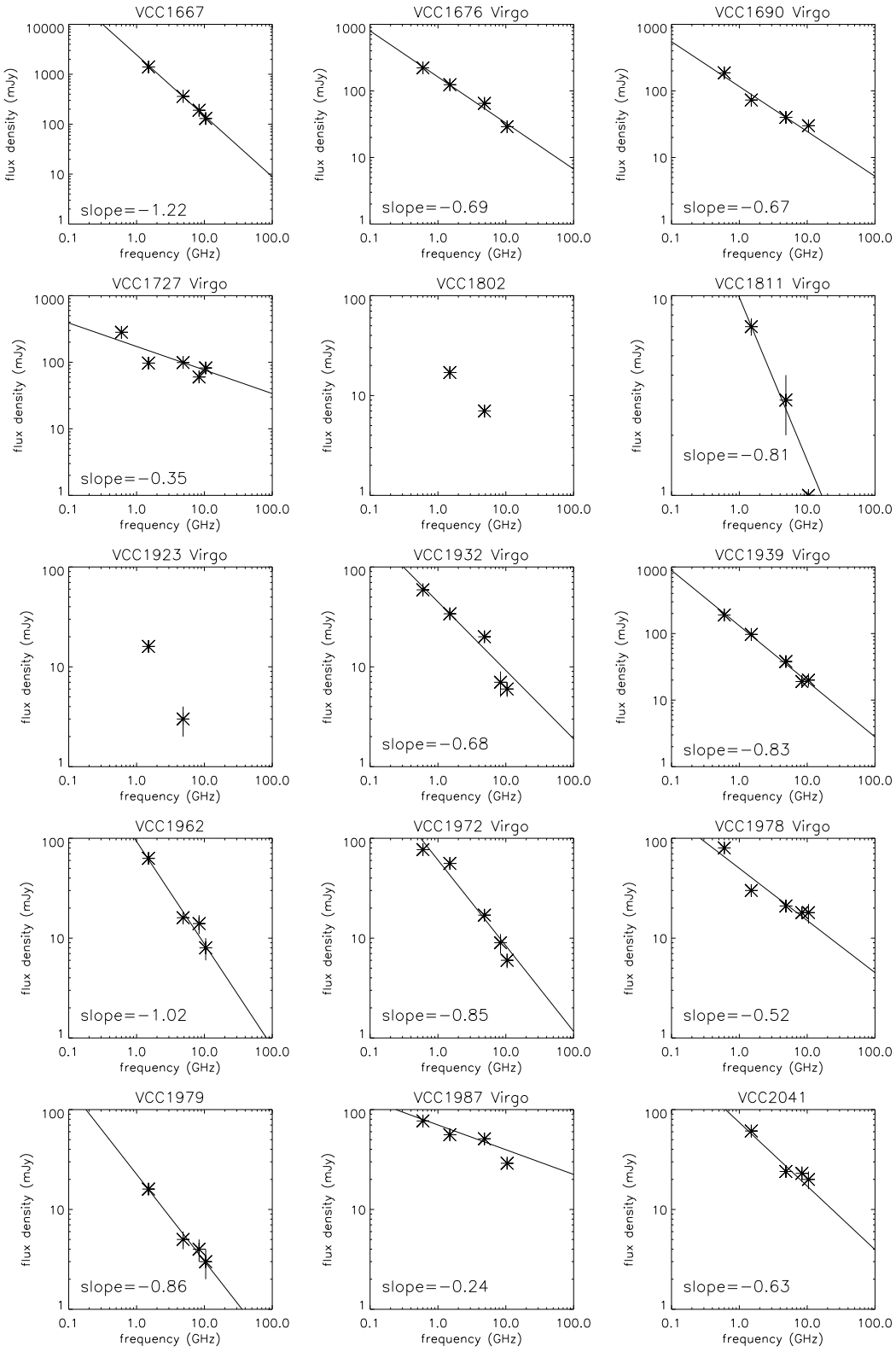

Fig. 3. Radio spectra of the observed VCC sources (continued).

radio excess, i.e. the absolute radio excess divided by the expected radio flux density calculated using the radio-FIR correlation. All four galaxies cited above have a relative radio excess greater than 2. Additionally, this is also the case for VCC0222 (NGC 4235, Sy1) and VCC1978. Thus, only galaxies that host an active center show a radio excess.

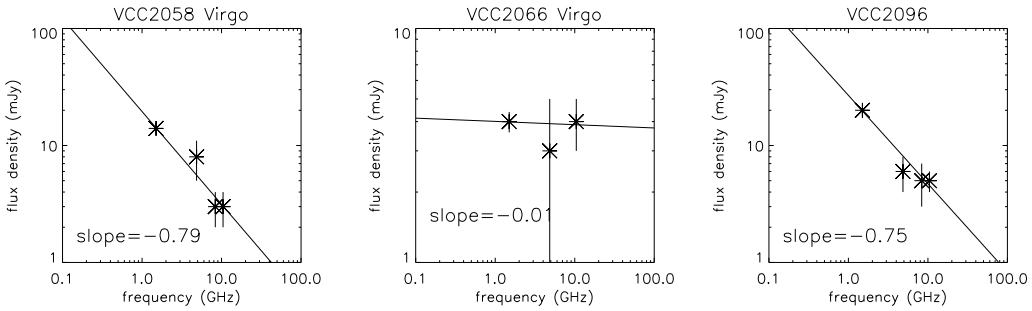

Fig. 3. Radio spectra of the observed VCC sources (continued).

6. The spectral index distribution

The distribution of the spectral index of the Virgo galaxies as a function of the projected distance to the cluster center (M87) can be seen in Fig. 6. Elliptical galaxies are represented as triangles. The galaxies with a spectral index greater than -0.5 are labeled. They are all spiral or S0 galaxies. VCC0222 is classified as a Sy1, VCC1110 as a LINER, and VCC1727 as a Sy2. The spectral index of VCC1200 has to be taken with some caution, because the 8.6 GHz flux density might be overestimated. VCC1450, VCC1535 and VCC1987 do not show any particular central activity. It might be worth noting that VCC1987 (NGC 4654) has most probably undergone a tidal interaction and is experiencing ram pressure now (Vollmer 2003). Moreover, it shows an off-center molecular bar (Sofue et al. 2003). So one could speculate that it is just developing a central activity. The galaxies with a spectral index > -0.5 are not concentrated towards the cluster center. Thus there is no indication that cluster environment leads to flatter spectral indices via central activity nor to steeper spectra as expected from better confinement of relativistic electrons. There might be a weak trend that the dispersion of the spectral index increases with decreasing projected distance to the cluster center. The steepest spectral indices $\alpha < -1.0$ are found in Sc/Scd galaxies and the elliptical galaxy VCC0763.

The number distribution of the spectral index is shown in Fig. 7. The dashed line traces the distribution of all sample galaxies, the solid line that of the Virgo cluster members. Both distributions peak around a spectral index of $\alpha = -0.9$. Both distributions show a tail to larger spectral indices than the peak value. The steepest spectra $\alpha < -1.2$ are found outside the Virgo cluster.

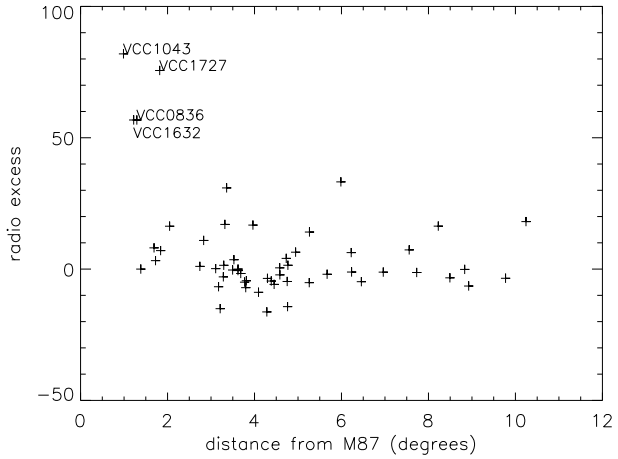

Fig. 5. Radio excess over the radio-FIR correlation of the observed VCC galaxies as a function of the projected distance to the cluster center (M87).

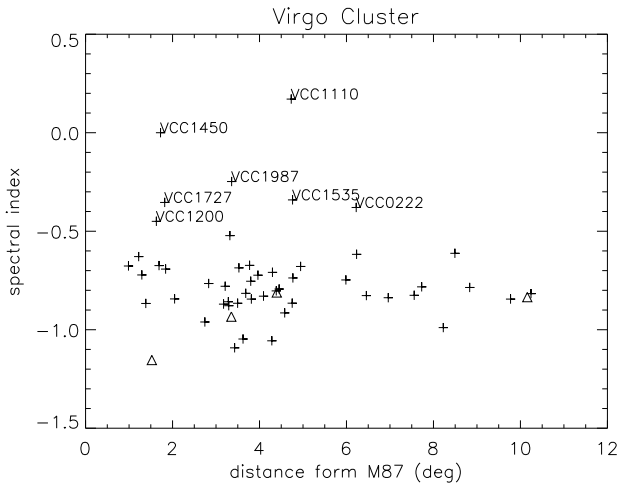

Fig. 6. Spectral index of the Virgo galaxies as a function of the projected distance to the cluster center (M87).

7. Discussion and Conclusions

We confirm the finding of Gavazzi & Boselli (1999b) that Virgo cluster galaxies statistically do not show an enhanced radio emission compared to isolated galaxies. However, a few spiral galaxies show an excess in the absolute radio/FIR ratio. These galaxies all possess active centers (LINER, HII, AGN) and are located within a radius of 2^o from the cluster center. We confirm the conclusion of Niklas et al. (1995) based on a small number of galaxies that the spectral index of Virgo galaxies does not change significantly with projected cluster distance. There might

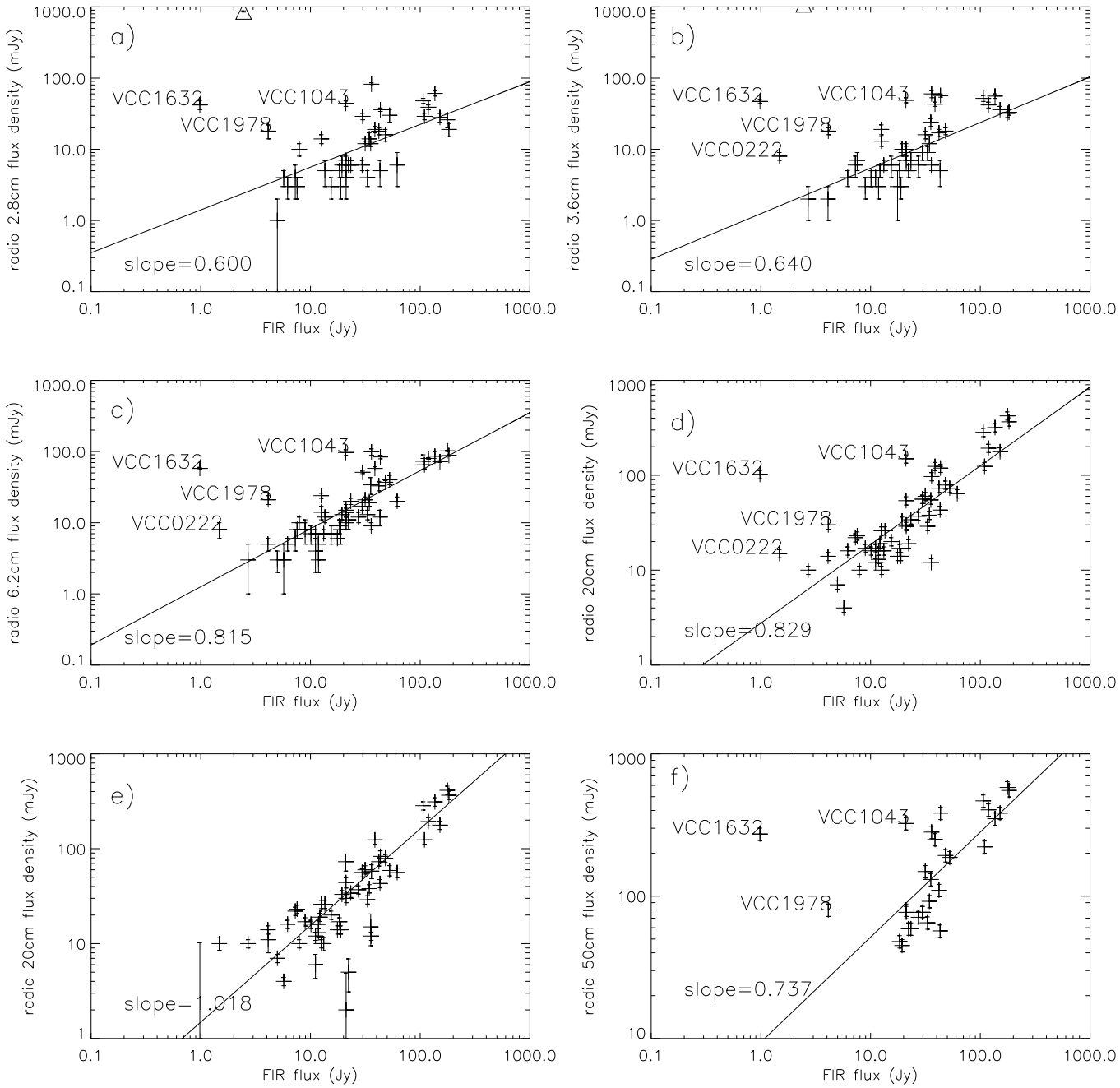

Fig. 4. Radio–FIR correlation: (a) at 10.55 GHz, (b) at 8.6 GHz, (c) at 4.85 GHz, (d) at 1.4 GHz (NVSS) (e) at 1.4 GHz FIRST central point source flux densities subtracted, (f) at 0.6 GHz.

be a trend that the scatter of the spectral indices with decreasing projected distance. The change in the behaviour of radio sources within the Virgo cluster (radio excess and spectral index) is due to central activity. It is not clear if and under which conditions the cluster environment triggers central activity.

As described in Sect. 1, during the phase of active ram pressure stripping, the magnetic field is compressed and one expects an excess of radio emission with respect to the FIR emission. This extended radio emission should be asymmetric in the outer parts of the disk. This seems not to be the case in the Virgo cluster. Based on the HI observations of the brightest spiral galaxies (Cayatte et al. 1990), no clear case for active ram pressure stripping could be identified. The only possible case is VCC1043 (NGC 4438), but there the galaxy had also a strong tidal interaction (Combes et al. 1988). A clearer case is the edge-on galaxy VCC1516 (NGC 4522) where high column density extraplanar HI is detected (Kenney et al. 2003, in prep.). Both galaxies do not show an enhanced, asymmetric radio continuum emission. However, in VCC1516 the compression is visible as a region of enhanced polariza-

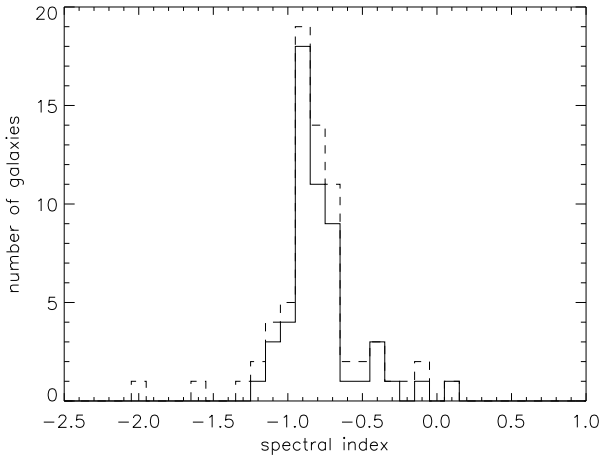

Fig. 7. Number distribution of the spectral index. Solid line: Virgo galaxies. Dashed line: all sample galaxies.

tion. In barred galaxies the situation is similar. Whereas in the compression upstream regions of the bar the radio polarization is enhanced, an excess of total radio continuum emission is not observed (Beck et al. 2001). We might speculate that this is the case, because both galaxies are stripped almost face-on, in which case the asymmetric compression is minimum. Other possibilities are: (i) the turbulent magnetic field is enhanced via an enhanced stars formation rate due to compression. The enhancement of the ordered magnetic field due to compression might then be negligible with respect to the turbulent magnetic field, but it can still be observed in polarization. (ii) During compression the scale height of the magnetic field increases, which leads to a decrease of the total magnetic field strength.

In the Coma cluster the situation is different. HI observations of the brightest spiral galaxies revealed highly asymmetric gas disks of high column density (Bravo-Alfaro et al. 2000). At the same time, Gavazzi & Boselli (1999b) found a statistical excess of radio emissivity for Coma cluster galaxies. This is a puzzling result, because the Virgo cluster is dynamical young (asymmetric galaxy distribution, constant velocity distribution of spirals), whereas the Coma cluster is more relaxed. One would thus expect that ram pressure is more active in the Virgo cluster. The solution to this paradigm is that the core radius of the Virgo cluster ICM distribution is much smaller than that of the Coma cluster. Thus Virgo galaxies have to come very close to the cluster center to be significantly stripped (Vollmer et al. 2001). In this case the phase of active ram pressure stripping is much shorter in the Virgo cluster than in the Coma cluster due to the small ICM core radius and the high galaxy velocities near the cluster center.

References

Beck R., Shoutenkov V., Ehle M., et al. 2002, A&A, 391, 83
Bothun G., Schommer R.A., Sullivan W.T.III, 1982, AJ, 87, 731
Cayatte V., van Gorkom J.H., Balkowski C., Kotanyi C., 1990, AJ, 100, 604
Cayatte V., Kotanyi C., Balkowski C., van Gorkom J.H., 1994, AJ, 107, 1003
Chamaraux P., Balkowski C., Gérard E., 1980, A&A, 83, 38
Combes F., Dupraz C., Casoli F., & Pagani L. 1988, A&A, 203, L9
Binggeli B., Sandage A., Tammann G., 1985, AJ 90, 1681 (VCC)
Bravo-Alfaro H., Cayatte V., van Gorkom J.H., & Balkowski C. 2000, AJ, 119, 580
de Jong T., Klein U., Wielebinski R., & Wunderlich E. 1985, A&A, 147, L6
Gavazzi G., 1987, ApJ, 320, 96
Gavazzi G., 1989, ApJ, 346, 59
Gavazzi G. & Boselli A. 1999a, A&A, 343, 86
Gavazzi G. & Boselli A. 1999b, A&A, 343, 93
Gavazzi G., Boselli A., Donati A., Franzetti P., & Scodeggio M. 2003, A&A, 400, 451
Giovanelli R., Haynes M.P., 1985, ApJ, 292, 404
Gunn J.E., Gott J.R., 1972, ApJ, 176, 1
Kotanyi C., van Gorkom J.H., & Ekers R.D. 1983, ApJ, 273, L7
Niklas S., Klein U., & Wielebinski R. 1995, A&A, 293, 56
Niklas S. 1997, A&A, 322, 29
Otmianowska-Mazur K. & Vollmer B. 2003, A&A, 402, 879
Ott M., Witzel A., Quirrenbach A., et al. 1994, A&A, 284, 331
Sofue Y., Koda J., Nakanishi H., et al. 2003, PASJ, 55, 17
Vollmer B., Cayatte V., Balkowski C., & Duschl W. J. 2001, ApJ, 561, 708
Vollmer B. 2003, A&A, 398, 525
Wunderlich E., Wielebinski R., & Klein U. 1987, A&A, 69, 487

Table 3. Radio and FIR fluxes of the galaxy sample.

Name	RA(B1950)	DEC(B1950)	D (deg.)	type	Virgo	$S^a_{2.8}$ (mJy)	$S^a_{3.6}$ (mJy)	$S^a_{6.2}$ (mJy)	S^b_{20} (mJy)	S^b_{50} (mJy)	S^c_{FIR} (Jy)	α
VCC0025	12 08 04	16 18 39	6.23	Sc	y	6 ± 2	10 ± 2	13 ± 2	33	45	19.35	−0.61
VCC0066	12 10 13	11 08 47	4.76	Sc	y	5 ± 2	–	12 ± 2	26	–	13.52	−0.73
VCC0073	12 10 29	07 19 00	6.96	Sb	y	4 ± 2	9 ± 2	14 ± 2	30	77	21.11	−0.83
VCC0089	12 11 15	13 42 11	4.38	Sc	y	5 ± 1	5 ± 2	9 ± 2	17	48	18.40	−0.80
VCC0092	12 11 15	15 10 32	4.94	Sb	y	$\mathbf{18 \pm 2}$	17 ± 2	$\mathbf{33 \pm 5}$	73	110	41.99	−0.67
VCC0120	12 12 05	06 05 06	7.72	Scd	y	–	4 ± 1	7 ± 2	16	–	10.09	−0.78
VCC0152	12 12 57	09 51 45	4.75	Scd	y	3 ± 1	6 ± 2	7 ± 2	20	–	15.41	−0.86
VCC0154	12 13 01	14 13 14	4.12	E/S0	n	12 ± 2	16 ± 3	19 ± 3	34	–	–	−0.50
VCC0157	12 13 05	14 10 41	4.09	Sc	y	4 ± 1	9 ± 2	13 ± 2	29	65	33.03	−0.82
VCC0167	12 13 21	13 25 38	3.81	Sb	y	–	3 ± 1	5 ± 2	13	–	11.81	−0.84
VCC0222	12 14 36	07 28 09	6.22	Sa	y	–	8 ± 1	8 ± 2	15	–	1.47	−0.37
VCC0224	12 14 35	12 43 57	3.42	Scd	y	16 ± 2	22 ± 2	42 ± 2	139	–	–	−1.09
VCC0302	12 16 09	12 00 24	3.10	Sc	n	–	2 ± 1	3 ± 2	10	–	2.69	−0.95
VCC0307	12 16 17	14 41 29	3.62	Sc	y	19 ± 4	33 ± 3	88 ± 2	366	553	182.45	−1.04
VCC0311	12 16 21	13 11 25	3.03	E/S0	n	–	9 ± 3	12 ± 2	12	–	–	−0.07
VCC0382	12 17 22	05 37 16	7.55	Sc	y	16 ± 3	18 ± 2	37 ± 2	79	193	48.16	−0.82
VCC0403	12 17 44	10 36 08	3.35	dE	y	13 ± 4	19 ± 2	33 ± 2	94	–	–	−0.93
VCC0414	12 17 51	14 58 12	3.48	dE	y	–	6 ± 1	–	14	–	–	
VCC0435	12 18 15	17 17 36	5.26	S	n	–	19 ± 3	24 ± 2	26	–	12.52	−0.12
VCC0437	12 18 15	17 46 12	5.68	dE	y	–	–	5 ± 1	15	–	–	
VCC0460	12 18 40	18 39 34	6.45	Sa	y	6 ± 1	5 ± 1	11 ± 3	19	59	22.20	−0.82
VCC0483	12 19 00	14 52 58	3.21	Sc	y	5 ± 2	5 ± 2	12 ± 3	43	57	42.99	−0.77
VCC0491	12 19 08	11 46 39	2.45	Scd	y	–	5 ± 1	–	19	–	12.17	
VCC0497	12 19 10	14 52 22	3.17	Sc	y	–	6 ± 2	12 ± 2	37	71	27.34	−0.87
VCC0508	12 19 21	04 45 03	8.22	Sc	y	26 ± 6	32 ± 4	102 ± 2	423	580	176.47	−0.98
VCC0559	12 19 59	15 48 54	3.77	Sab	y	–	4 ± 1	4 ± 2	12	–	11.10	−0.67
VCC0572	12 20 09	03 25 06	9.47	E/S0	n	–	7 ± 1	6 ± 2	14	–	–	−0.42
VCC0580	12 20 12	12 34 15	2.02	BCD	n	–	4 ± 2	5 ± 1	21	–	–	−1.13
VCC0596	12 20 22	16 06 01	3.96	Sc	y	$\mathbf{61 \pm 5}$	56 ± 4	$\mathbf{86 \pm 14}$	318	350	136.00	−0.72
VCC0638	12 20 50	07 45 00	5.25	Sab	n	7 ± 1	7 ± 2	10 ± 2	29	–	21.11	−0.76
VCC0763	12 22 31	13 09 12	1.52	E	y	864 ± 15	1085 ± 20	2270 ± 20	6067	10802	2.45	−1.15
VCC0801	12 22 53	16 44 47	4.29	Sa	y	14 ± 3	12 ± 3	19 ± 2	38	92	34.36	−0.70
VCC0831	12 23 10	09 18 29	3.59	Sc	n	5 ± 1	8 ± 2	12 ± 2	25	–	–	−0.74
VCC0836	12 23 14	12 56 20	1.29	Sab	y	$\mathbf{36 \pm 2}$	57 ± 3	$\mathbf{84 \pm 5}$	119	383	43.32	−0.72
VCC0865	12 23 27	15 56 49	3.49	Sc	y	4 ± 2	6 ± 2	6 ± 2	22	–	7.26	−0.86
VCC0873	12 23 34	13 23 24	1.38	Sc	y	$\mathbf{12 \pm 1}$	16 ± 2	$\mathbf{21 \pm 2}$	60	149	31.48	−0.86
VCC0904	12 23 55	09 17 54	3.54	Pec	n	9 ± 3	12 ± 4	42 ± 2	404	–	–	−1.94
VCC0907	12 23 55	09 17 49	3.54	Pec	n	11 ± 3	11 ± 3	45 ± 2	257	–	–	−1.56
VCC0921	12 24 02	04 14 29	8.49	Sbc	y	–	6 ± 1	7 ± 1	16	–	13.18	−0.61
VCC0958	12 24 24	15 19 28	2.82	Sa	y	$\mathbf{12 \pm 1}$	24 ± 3	$\mathbf{34 \pm 9}$	55	131	35.38	−0.76
VCC1040	12 25 10	13 15 22	0.97	dE	y	–	3 ± 1	–	17	–	–	
VCC1043	12 25 13	13 17 07	0.98	Sb	y	$\mathbf{44 \pm 4}$	49 ± 4	$\mathbf{97 \pm 9}$	149	324	20.97	−0.67
VCC1110	12 25 58	17 21 38	4.72	Sab	y	$\mathbf{14 \pm 2}$	13 ± 2	14 ± 3	10	–	12.55	0.17
VCC1145	12 26 25	03 50 49	8.83	Sb	y	–	10 ± 2	15 ± 3	54	80	21.06	−0.78
VCC1200	12 27 02	11 04 10	1.62	Im	y	–	4 ± 2	9 ± 2	13	–	–	−0.44
VCC1205	12 27 05	08 05 53	4.57	Sc	y	–	3 ± 1	8 ± 3	17	–	8.94	−0.91
VCC1226	12 27 14	08 16 39	4.39	E/S0	y	42 ± 3	52 ± 3	84 ± 3	248	392	–	−0.81
VCC1376	12 29 07	04 12 13	8.46	Sc	n	6 ± 2	4 ± 1	10 ± 3	17	–	–	−0.68
VCC1393	12 29 24	15 23 46	2.74	Sc	y	–	2 ± 1	5 ± 1	14	–	4.08	−0.96
VCC1401	12 29 27	14 41 38	2.04	Sbc	y	$\mathbf{48 \pm 4}$	52 ± 5	$\mathbf{73 \pm 17}$	284	467	106.37	−0.84
VCC1413	12 29 35	12 41 59	0.32	dE	y	–	–	–	43	–	–	
VCC1449	12 30 08	13 35 35	1.03	dE	y	–	–	–	20	–	–	

[a] this paper and measurements of Niklas et al. (1995) in boldface
[b] from Goldmine (Gavazzi et al. 2003)

Table 3. Radio and FIR fluxes of the galaxy sample (continued).

Name	RA(B1950)	DEC(B1950)	D (deg.)	type	Virgo	$S^a_{2.8}$ (mJy)	$S^a_{3.6}$ (mJy)	$S^a_{6.2}$ (mJy)	S^b_{20} (mJy)	S^b_{50} (mJy)	S^c_{FIR} (Jy)	α
VCC1450	12 30 10	14 19 35	1.72	Sc	y	**10 ± 2**	–	10 ± 2	10	–	7.87	0.00
VCC1508	12 30 58	08 55 43	3.79	Sc	y	–	3 ± 2	6 ± 1	14	–	17.60	−0.75
VCC1516	12 31 07	09 27 03	3.29	Sbc	y	3 ± 1	7 ± 2	8 ± 2	23	–	7.55	−0.87
VCC1535	12 31 30	07 58 30	4.76	S0	y	–	6 ± 1	9 ± 1	12	–	35.75	−0.34
VCC1540	12 31 35	02 55 46	9.77	Sb	y	28 ± 4	36 ± 4	72 ± 2	177	383	151.21	−0.84
VCC1554	12 31 46	06 44 40	5.98	Sm	y	**19 ± 2**	43 ± 3	**58 ± 3**	124	250	38.60	−0.74
VCC1555	12 31 47	08 28 25	4.28	Sc	y	6 ± 3	–	20 ± 3	64	–	61.62	−1.05
VCC1562	12 31 53	02 27 50	10.2	Sc	y	39 ± 3	42 ± 4	80 ± 2	193	404	118.57	−0.81
VCC1632	12 33 08	12 49 53	1.22	S0	y	42 ± 6	47 ± 3	58 ± 2	102	273	0.98	−0.62
VCC1658	12 33 45	13 51 07	1.80	dE	y	–	–	3 ± 2	11	–	–	
VCC1667	12 33 58	16 49 02	4.38	dE	n	130 ± 8	190 ± 10	360 ± 10	1402	–	–	−1.22
VCC1673	12 33 59	11 32 01	1.81	Sc	y	–	–	–	10	–	–	–
VCC1676	12 34 02	11 30 55	1.84	Sc	y	**29 ± 3**	–	**65 ± 8**	124	222	109.33	−0.69
VCC1690	12 34 18	13 26 27	1.68	Sab	y	**30 ± 6**	–	**40 ± 6**	73	187	52.60	−0.67
VCC1727	12 35 12	12 05 37	1.81	Sab	y	**82 ± 4**	60 ± 7	**99 ± 10**	97	282	35.95	−0.35
VCC1802	12 37 06	07 26 36	5.66	S	n	–	–	7 ± 1	17	–	11.09	
VCC1811	12 37 21	15 34 20	3.68	Sc	y	**1 ± 1**	–	3 ± 1	7	–	4.99	−0.81
VCC1923	12 39 59	04 14 05	8.92	Sbc	y	–	–	3 ± 1	16	–	11.83	
VCC1932	12 40 10	14 34 12	3.52	Sc	y	**6 ± 1**	7 ± 2	**20 ± 2**	34	59	23.30	−0.68
VCC1939	12 40 17	02 57 43	10.1	E/S0	y	20 ± 4	19 ± 2	38 ± 3	97	190	–	−0.83
VCC1962	12 40 45	03 49 26	9.37	S0	n	8 ± 2	14 ± 3	16 ± 2	63	–	–	−1.02
VCC1972	12 41 01	11 51 23	3.28	Sc	y	**6 ± 1**	9 ± 2	17 ± 2	56	77	29.58	−0.85
VCC1978	12 41 08	11 49 34	3.31	S0	y	18 ± 4	18 ± 2	21 ± 3	30	80	4.11	−0.52
VCC1979	12 41 14	11 02 37	3.61	Sc	n	3 ± 1	4 ± 1	5 ± 1	16	–	6.18	−0.86
VCC1987	12 41 24	13 24 10	3.35	Sc	y	**29 ± 3**	–	**51 ± 2**	56	77	29.84	−0.24
VCC2041	12 44 02	12 10 09	3.96	E/S0	n	20 ± 4	23 ± 4	24 ± 2	61	–	–	−0.63
VCC2058	12 45 14	14 02 05	4.45	Sc	y	**3 ± 1**	3 ± 1	**8 ± 3**	14	–	18.87	−0.79
VCC2066	12 45 44	11 15 22	4.58	S0	y	**4 ± 1**	–	**3 ± 2**	4	–	5.69	−0.01
VCC2096	12 50 54	11 58 54	5.69	BCD	n	**5 ± 1**	5 ± 2	**6 ± 2**	20	–	–	−0.75

[a] this paper and measurements of Niklas et al. (1995) in boldface
[b] from Goldmine (Gavazzi et al. 2003)